Modulation of sensory information processing by a neuroglobin in *Caenorhabditis elegans*

Shigekazu Oda[a,1,2], Yu Toyoshima[b], and Mario de Bono[a,1]

[a]Division of Cell Biology, Medical Research Council Laboratory of Molecular Biology, Cambridge CB2 0QH, United Kingdom; and [b]Department of Biological Sciences, Graduate School of Science, University of Tokyo, Tokyo 113-0033, Japan

Edited by Iva Greenwald, Columbia University, New York, NY, and approved April 25, 2017 (received for review August 31, 2016)

Sensory receptor neurons match their dynamic range to ecologically relevant stimulus intensities. How this tuning is achieved is poorly understood in most receptors. The roundworm *Caenorhabditis elegans* avoids 21% O_2 and hypoxia and prefers intermediate O_2 concentrations. We show how this O_2 preference is sculpted by the antagonistic action of a neuroglobin and an O_2-binding soluble guanylate cyclase. These putative molecular O_2 sensors confer a sigmoidal O_2 response curve in the URX neurons that has highest slope between 15 and 19% O_2 and approaches saturation when O_2 reaches 21%. In the absence of the neuroglobin, the response curve is shifted to lower O_2 values and approaches saturation at 14% O_2. In behavioral terms, neuroglobin signaling broadens the O_2 preference of *Caenorhabditis elegans* while maintaining avoidance of 21% O_2. A computational model of aerotaxis suggests the relationship between GLB-5–modulated URX responses and reversal behavior is sufficient to broaden O_2 preference. In summary, we show that a neuroglobin can shift neural information coding leading to altered behavior. Antagonistically acting molecular sensors may represent a common mechanism to sharpen tuning of sensory neurons.

sensory neuron tuning | neural coding | oxygen sensing | neuroglobin | computational model

The response properties of sensory neurons can be characterized by tuning curves that relate stimulus parameters to the evoked response (1, 2). Some sensory neurons show dynamic ranges that span several orders of stimulus magnitude (e.g., odor concentration), whereas others show remarkably narrow tuning curves. For example, glomus cells of the carotid body show oxygen-evoked responses that are tuned to a twofold to threefold change in O_2 levels at the physiologically appropriate O_2 concentration range (3, 4). How such sharp tuning is achieved is poorly understood.

Neuroglobins are members of the globin family of heme-binding proteins expressed mainly in neurons (5). They have been described throughout metazoa, from cnidarians to man (6). Their physiological functions are unclear. They have been proposed to metabolize reactive oxygen species (ROS), signal redox state, store O_2, control apoptosis, and negatively regulate Gi/o signaling (7). The genome of *Caenorhabditis elegans* encodes an unusually large family of globins, and many are expressed in neurons (8). One of these, GLOBIN-5 (GLB-5), is expressed in the oxygen sensing neurons URX, AQR, PQR, and BAG, where it accumulates at dendritic endings (9, 10). *C. elegans* avoids both normoxia (21% O_2) and hypoxia (11). Avoidance of 21% O_2 enables the animal to escape the surface and is mediated by O_2 receptors, most importantly the *glb-5*–expressing URX, AQR, and PQR neurons (12). Like vertebrate neuroglobins, GLB-5 has the spectroscopic fingerprints of a hexa-coordinated heme iron and rapidly oxidizes to the ferric state in normoxia (9). The *glb-5* gene is defective in the domesticated reference strain of *C. elegans*, N2 (Bristol), but natural isolates encode a functional allele, *glb-5(Haw)* (9, 10) (*Haw* refers to Hawaii, the geographical origin of the natural isolate in which this allele was first described). Behavioral and Ca^{2+} imaging studies suggest that functional GLB-5 alters the properties of the O_2 receptors and *C. elegans'* O_2 responses (9, 10). However, how GLB-5 alters the representation of environmental information in these neurons leading to behavioral change is unknown.

The URX O_2 receptors exhibit phasic–tonic signaling properties and, in response to changes in O_2 concentration, evoke both transient behavioral responses that are coupled to the rate of change of O_2, dO_2/dt, and more persistent behavioral responses coupled to O_2 levels (8, 13). The transient responses are reversals and turns that allow *C. elegans* to navigate O_2 gradients. The sustained responses involve persistent changes in the rate of movement that enable feeding animals to escape 21% O_2 or to accumulate in preferred lower O_2 environments. Besides GLB-5, the URX neurons express another putative molecular O_2 sensor, a soluble guanylate cyclase composed of GCY-35 and GCY-36 (guanylate cyclase) subunits (11, 13, 14). These soluble guanylate cyclases have a heme–nitric oxide/oxygen (H-NOX) binding domain that appears to stimulate cGMP production upon binding molecular O_2 (10, 11). Recent work suggests mammalian soluble guanylate cyclases also mediate O_2 sensing in glomus cells of the carotid body, although they do not bind O_2 (15). Here we show that the GLB-5 neuroglobin and soluble guanylate cyclases work antagonistically to confer on URX a sigmoidal O_2 stimulus–response curve that has its steepest slope between 15 and 19% O_2 and begins to plateau as O_2 levels approach 21%. By tuning URX, GLB-5 broadens the range of O_2 environments preferred by *C. elegans*. Using computer modeling we show that this altered preference can be explained by changes in how URX evokes reversals in response to O_2 stimuli.

Significance

Sensory neurons encode environmental stimuli in their electrical activity and alter behavior and physiology by transmitting this information to downstream circuits. Their response properties can be characterized by tuning curves that relate stimulus parameters to neural responses. Tuning curves identify the response threshold, the stimulus features at the tuning curve peak, and high-slope regions that give maximum stimulus discrimination. Here we show that two antagonistically acting molecular oxygen sensors, a neuroglobin and a soluble guanylate cyclase, sculpt a sharp sigmoidal tuning curve in the URX oxygen sensing neurons of *Caenorhabditis elegans*. By combining experiments with computational modelling, we show that these changes in stimulus-encoding properties broaden *C. elegans*'s O_2 preference.

Author contributions: S.O., Y.T., and M.d.B. designed research; S.O. and Y.T. performed research; S.O., Y.T., and M.d.B. analyzed data; and S.O., Y.T., and M.d.B. wrote the paper.

The authors declare no conflict of interest.

This article is a PNAS Direct Submission.

Freely available online through the PNAS open access option.

[1]To whom correspondence may be addressed. Email: debono@mrc-lmb.cam.ac.uk or shigeoda@11.alumni.u-tokyo.ac.jp.

[2]Present address: Division of Quantitative Biology, Okazaki Institute for Integrative Bio-sciences, National Institutes of Natural Sciences, Okazaki, Aichi 444-8787, Japan.

This article contains supporting information online at www.pnas.org/lookup/suppl/doi:10.1073/pnas.1614596114/-/DCSupplemental.

Results

The GLB-5 Allele in Natural Isolates Broadens *C. elegans*'s O_2 Preference. Previous studies of *glb-5* used a loss-of-function allele that arose in the N2 laboratory strain during domestication (9, 10, 16). This allele, *glb-5(N2)*, is a partial duplication that generates multiple splice isoforms, and it is unclear if it abolishes *glb-5* function. We therefore compared animals bearing the *glb-5(Haw)* functional allele to mutants carrying a predicted null mutation, *glb-5(tm5440)*, which deletes part of the globin domain and introduces a premature stop codon. To analyze how the GLB-5 neuroglobin alters O_2 preference we compared the distribution of *glb-5(Haw)* and *glb-5(tm5440)* animals in a shallow 0–21% O_2 gradient in the presence of food. Unless otherwise indicated, in our experiments we used strains defective in the neuropeptide receptor *npr-1*, because besides harboring a defective *glb-5* allele, the N2 laboratory strain has acquired a gain-of-function mutation in *npr-1* that confers O_2-sensing defects (11). *glb-5(tm5440); npr-1* animals accumulated in a narrow range of O_2 concentrations, between 7 and 10% O_2 (Fig. 1 *A* and *B*). By contrast, animals bearing the natural *glb-5(Haw)* allele distributed over a broader range of O_2 concentrations, between 17 and 5% O_2, but still avoided 21% O_2 and hypoxia (Fig. 1 *A* and *B*). These behavioral data imply that the GLB-5(Haw) neuroglobin changes how O_2-sensing neurons respond in O_2 gradients.

GLB-5 Changes the Dynamic Range of the URX O_2 Sensor. We used the GCaMP6s Ca^{2+} sensor to examine how functional *glb-5* alters neural coding of O_2 levels in the URX O_2 sensors (17). The dynamics of the Ca^{2+} responses evoked in URX by a 7–21% O_2 step stimulus did not differ significantly between *glb-5(tm5440)* and *glb-5(Haw)* animals (Fig. S1). However, the Ca^{2+} responses to a 7–19% O_2 exponential ramp stimulus differed markedly between these strains (Fig. 1*C*). In animals expressing *glb-5(Haw)*, Ca^{2+} in URX increased continuously as O_2 levels rose from 7 to 19%. By contrast, the Ca^{2+} responses of *glb-5(tm5440)* mutants appeared to plateau at ~14% O_2. As expected, the URX neurons did not respond to the O_2 stimulus in animals defective in both *glb-5* and the *gcy-35* soluble guanylate cyclase (Fig. 1*C*). This defect could be rescued by expressing wild-type *gcy-35* and *glb-5(Haw)* cDNA selectively in URX (Fig. S2 *A* and *B*). Selectively expressing wild-type *gcy-35* cDNA but *glb-5(Haw)* cDNA that contained a stop codon conferred URX responses that plateaued at ~14% O_2 (Fig. S2 *A* and *B*). These differences suggest that the GLB-5 neuroglobin changes the dynamic range of URX (Fig. 1*C*). The effect of *glb-5* alleles on the URX Ca^{2+} response was similar whether we imaged animals in the presence (Fig. 1*C*) or absence of food (Fig. S2 *C* and *D*).

To investigate further how the GLB-5 neuroglobin alters neural coding, we delivered different patterns of O_2 stimuli and imaged Ca^{2+} responses in URX. We focused on URX because these sensory neurons are sufficient for several O_2-coupled behaviors including aerotaxis and aggregation (18, 19) (Fig. S3). To plot the relationship between stimulus intensity and URX Ca^{2+} responses we sequentially increased the O_2 stimulus given to the same animal in 2% increments, returning to 7% O_2 between stimuli (Fig. 2*A*). In *glb-5(Haw)* animals URX neurons showed a higher O_2 response threshold than in *glb-5(tm5440)* mutants, as well as a

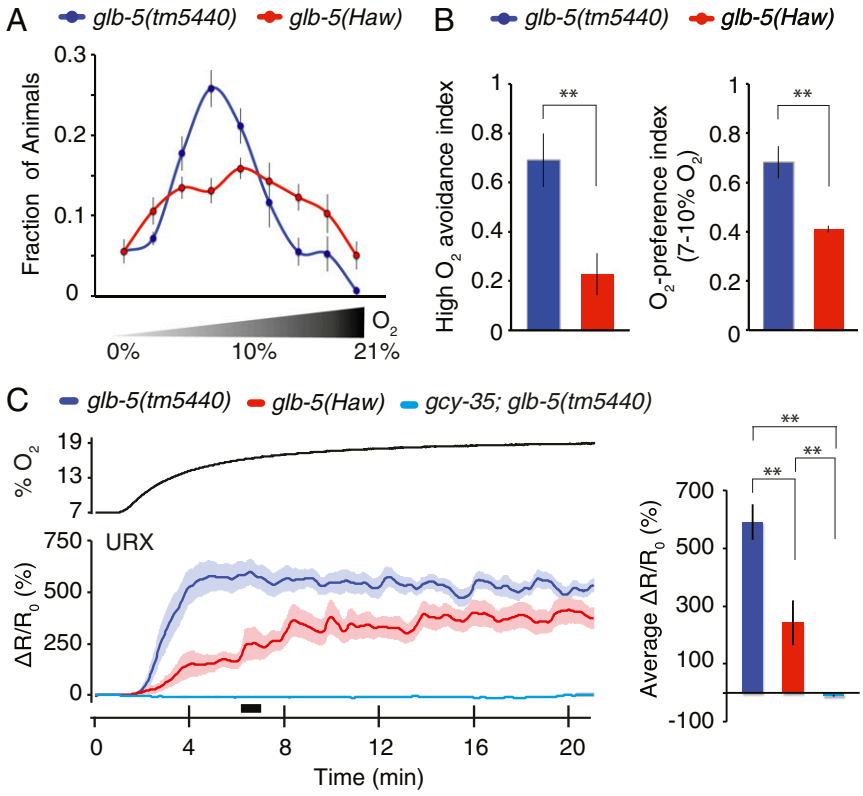

Fig. 1. The GLB-5 neuroglobin broadens *C. elegans*'s O_2 preference. (*A*) Aerotaxis behavior. Distribution of animals in a 0–21% O_2 gradient. $n = 6$. Plots show mean ± SEM. (*B*) The *glb-5(Haw)* allele broadens *C. elegans*'s O_2 preference. High O_2 avoidance index = (fraction of animals in 7–14% O_2) − (fraction of animals in 14–21% O_2)/(fraction of animals in 7–21% O_2). O_2 preference (7–10% O_2) = (fraction of animals in 7–10% O_2)/(fraction of animals in 7– 21% O_2). $^{**}P < 0.01$, Mann–Whitney *u* test. Data are from *A*. (*C*) Mean Ca^{2+} responses of URX neurons to the indicated O_2 ramp stimulus. $n = 9$–12. Shading represents SEM. The Ca^{2+} sensor is GCaMP6s coexpressed with mCherry (URX). Also shown are the responses of *gcy-35; glb-5(tm5440)* mutants; GCY-35 is required for measurable O_2-evoked Ca^{2+} responses. The color bars represent the average response for each genotype at time point indicated by the black bar. Data show mean ± SEM. $^{**}P < 0.01$, ANOVA with Tukey's post hoc test. The O_2 ramp stimulus (*Top*) shows the mean of four measurements ± SEM.

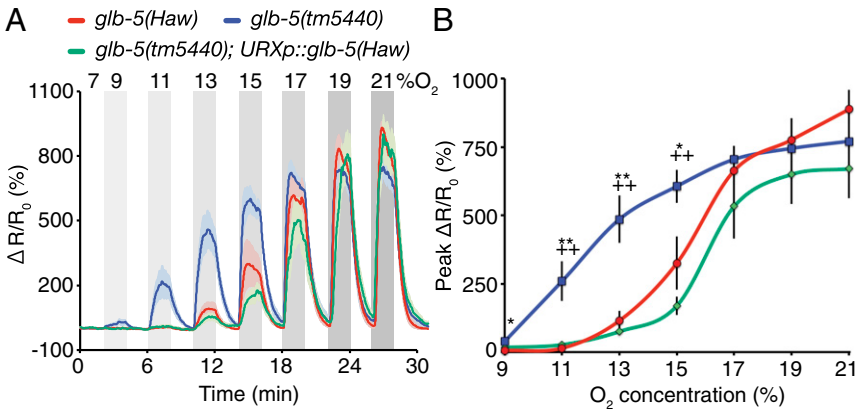

Fig. 2. GLB-5 changes the stimulus–response curve of O_2-evoked Ca^{2+} responses in URX. (*A*) Ca^{2+} responses evoked in URX by a graded series of O_2 steps that start from a 7% O_2 baseline ($n = 10$). Data show mean ± SEM. Responses are normalized to the GCaMP6s/mCherry ratio averaged over the 10 s before delivery of the stimulus train. (*B*) Maximum amplitude of the responses from *A* plotted against O_2 stimulus intensity. Bars represent SEM. $^*P < 0.05$; $^{**}P < 0.01$; *glb-5(Haw)* vs. *glb-5(tm5440)*. $^{++}P < 0.01$; *glb-5(tm5440) URXp::glb-5(Haw)* vs. *glb-5(tm5440)*. ANOVA with Dunnett's post hoc test.

steep sigmoidal O_2 response curve whose half maximum was at much higher O_2 concentrations (Fig. 2 *A* and *B*). Selectively expressing a *glb-5(Haw)* transgene in URX in *glb-5(tm5440)* mutants conferred a URX stimulus–response profile that closely resembled that of *glb-5(Haw)* animals (Fig. 2 *A* and *B*). Thus, GLB-5(Haw) cell-autonomously shifts the URX stimulus–response curve toward higher O_2 concentrations (Fig. 2*B*).

To extend these observations, we examined URX responses to a different set of stimuli in which we increased O_2 levels in 2% steps but varied the starting O_2 concentration and delivered only one stimulus per animal. Again, we observed that the *glb-5(Haw)* allele shifted the tuning curve of URX such that both the tonic Ca^{2+} levels at the new O_2 concentration and the change in Ca^{2+} normalized to the prestimulus Ca^{2+} level, $\Delta R/R_0$ (which is a measure of the response amplitude), gradually increased as O_2 approached 19–21% (Fig. 3 *A* and *B*). By contrast, in *glb-5(tm5440)* mutants, $\Delta R/R_0$ was at a maximum when animals experienced an 11 → 13% O_2 stimulus (Fig. 3 *A* and *B*). Expressing *glb-5(Haw)* cDNA selectively in URX in *glb-5(tm5440)* animals was sufficient to confer a *glb-5(Haw)*–like dose–response curve to this neuron under these stimulation conditions (Fig. 3 *A* and *B*).

Step stimulation is used widely to study the properties of sensory neurons, but in their natural environment, *C. elegans* likely also encounter slowly varying O_2 levels, similar to those encountered by animals in the aerotaxis assay (Fig. 1*A*). We therefore measured the Ca^{2+} responses evoked in URX by a set of 2% O_2 exponential ramp stimuli. Our results revealed a response pattern similar to that observed for the corresponding step stimulus (Fig. 3 *C* and *D*). In animals expressing the *glb-5(Haw)* allele, URX responses to ramp stimuli increased gradually as O_2 levels increased. By contrast, in *glb-5(tm5440)* mutants the URX response amplitudes, measured as $\Delta R/R_0$, showed a peak response to the 13 → 15% O_2 stimulus and were otherwise similar across the different ramp stimuli we delivered (Fig. 3 *C* and *D*). The response property changes conferred by GLB-5(Haw) are therefore robust to different O_2 stimulation patterns. Together, our Ca^{2+} imaging experiments suggest that GLB-5(Haw) alters neural encoding of O_2 stimuli in URX, shifting the dynamic range to higher O_2 concentrations and making it more sharply tuned.

cGMP Signaling in URX. In previous work we used the genetically encoded cGMP sensor cGi500 (20) to visualize cGMP dynamics in the PQR O_2-sensing neuron (14). We showed that a rise in O_2 stimulates a tonic rise in cGMP that requires the GCY-35 soluble guanylate cyclase and that the Ca^{2+} influx resulting from gating of cGMP channels feeds back to limit O_2-evoked rises in cGMP by stimulating cGMP hydrolysis (14) (Fig. S4*A*). We used the cGi500 sensor to examine if GLB-5(Haw) can modulate cGMP dynamics in URX. We could not detect O_2-evoked cGMP responses in the cell body of URX neurons unless we disrupted *cng-1*, which encodes a cGMP-gated channel subunit required for O_2-evoked Ca^{2+} responses in URX (Fig. S4 *A* and *B*). This suggests that URX and PQR have similar negative feedback control of cGMP accumulation. The cGMP responses evoked in URX by an exponential ramp O_2 stimulus were comparable in *glb-5(tm5440) cng-1* and *glb-5(Haw) cng-1* animals under our experimental conditions (Fig. 4 *B* and *C*). These results would suggest that GLB-5(Haw) does not alter URX neural coding by modulating cGMP levels, However, we cannot exclude the possibility that measuring cGMP in the cell body does not adequately report cGMP changes in the dendritic ending, where GLB-5, GCY-35/GCY-36, and the cGMP channels are localized.

GLB-5 Effects on URX Behavioral Outputs. How do the changes in URX information coding mediated by GLB-5(Haw) alter motor responses to O_2 stimuli? To address this question, we quantified behavioral responses to a range of O_2 stimuli, focusing on reversal in the direction of movement and changes in speed, both important features of O_2-evoked behaviors (18, 19). Avoidance of high O_2 levels is mediated principally by three sensory neurons, URX, PQR, and AQR, each of which expresses the GCY-35/36 O_2 receptor and GLB-5 (11–13, 18). To selectively study how URX output alters behavior we studied *gcy-35(ok769); glb-5(tm5440)* mutants that expressed *glb-5(Haw)* and/or *gcy-35* cDNA in URX but not AQR or PQR (*Methods*). Unexpectedly, only O_2 stimuli that evoked intermediate URX Ca^{2+} responses evoked strong reversals in these animals (Figs. 3 *A* and *B* and 4 *A* and *B*). O_2 stimuli that evoked either small or large URX Ca^{2+} responses failed to evoke reversals (Figs. 3 *A* and *B* and 4 *A* and *B*). We also observed this relationship between the Ca^{2+} response magnitude and reversals when we expressed *glb-5(Haw)* selectively in URX, although the O_2 range that evoked the reversals most strongly was different (Figs. 3 *A* and *B* and 4 *A* and *B*). These data suggest that URX associated circuits include a filter that prevents strong stimulation of URX from inducing reversals. Consistent with this, a 13 → 21% O_2 step stimulus that evoked a large URX Ca^{2+} response did not evoke reversals in animals expressing *gcy-35* selectively in URX (Fig. S5).

One important output for the URX O_2 sensors is the RMG interneurons, which are connected to URX by both synapses and gap junctions (21–23). O_2-evoked responses in RMG correlated well with those in URX when we stimulated animals expressing *gcy-35* selectively in URX with 13 → 15% and 13 → 21% O_2 steps

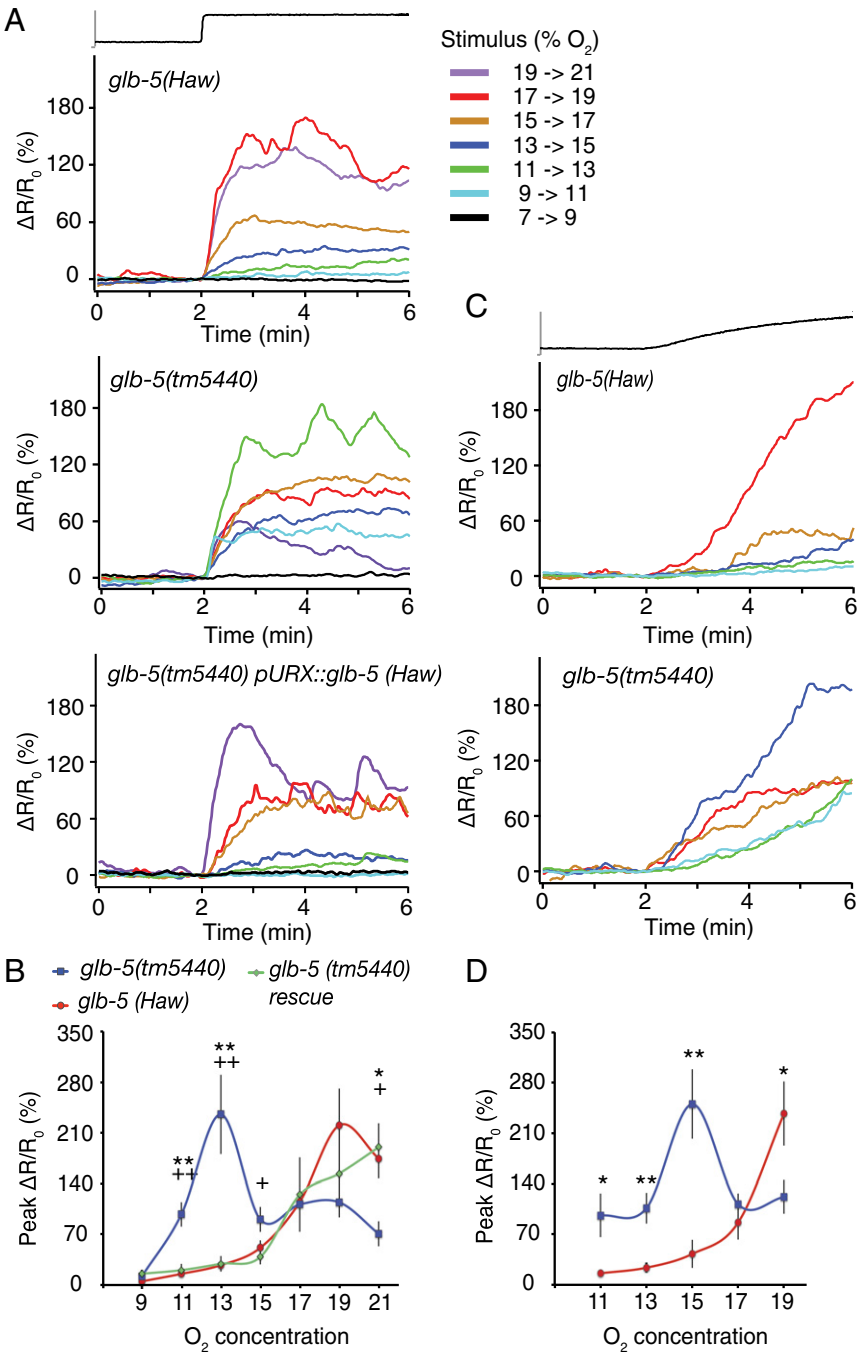

Fig. 3. Response properties of URX sensory neurons with and without GLB-5(Haw). (*A*) Averaged traces of the Ca^{2+} response of URX to different 2% O_2 step stimuli in the genotypes indicated. n = 12–18. (*B*) Maximum amplitudes of the responses shown in *A* plotted against stimulus intensity. Data show mean ± SEM. (*C*) Averaged traces of the Ca^{2+} response of URX to different 2% O_2 ramp stimuli in *glb-5(Haw)* and *glb-5(tm5440)* animals. n = 13–16. (*D*) Maximum amplitude of the responses shown in *C* plotted against stimulus intensity. Data show mean and SEM. The O_2 plots of a step and a ramp stimulus at the top of *A* and *C* show the mean of 9 (*A*) and 10 (*C*) measurements ± SEM. $^{*}P < 0.05$; $^{**}P < 0.01$; *glb-5(Haw)* vs. *glb-5(tm5440)*. $^{+}P < 0.05$; $^{++}P < 0.01$; *glb-5(tm5440) URXp::glb-5(Haw)* vs. *glb-5(tm5440)*. ANOVA with Dunnett's post hoc test (*B*). Mann–Whitney *u* test (*D*).

(Fig. S6). This suggests information transfer from URX to RMG does not explain the nonlinearity in the relationship between URX Ca^{2+} responses and reversals. URX output also stimulated locomotory speed when O_2 levels rose above 17% O_2 in both *glb-5(tm5440)* and *glb-5(Haw)* strains (Fig. 4 *C* and *D*). Together, our results suggest that information from URX is transmitted to both reversal and speed circuits; however, reversals can be evoked by changes in URX activity that evoke modest or no changes in speed.

A Computational Model for Aerotaxis. Using our detailed analyses of how URX responds to different O_2 stimuli, we carried out computational modeling experiments to ask if the relationship between URX activity and reversal behavior was sufficient to explain the altered O_2 preference of animals expressing *glb-5(Haw)*. To build a model for aerotaxis we incorporated the Ca^{2+} imaging data in Fig. 3*A* and the behavioral data in Fig. 4*C* (*Methods*). For simplicity, and because URX is sufficient for *C. elegans* to show an

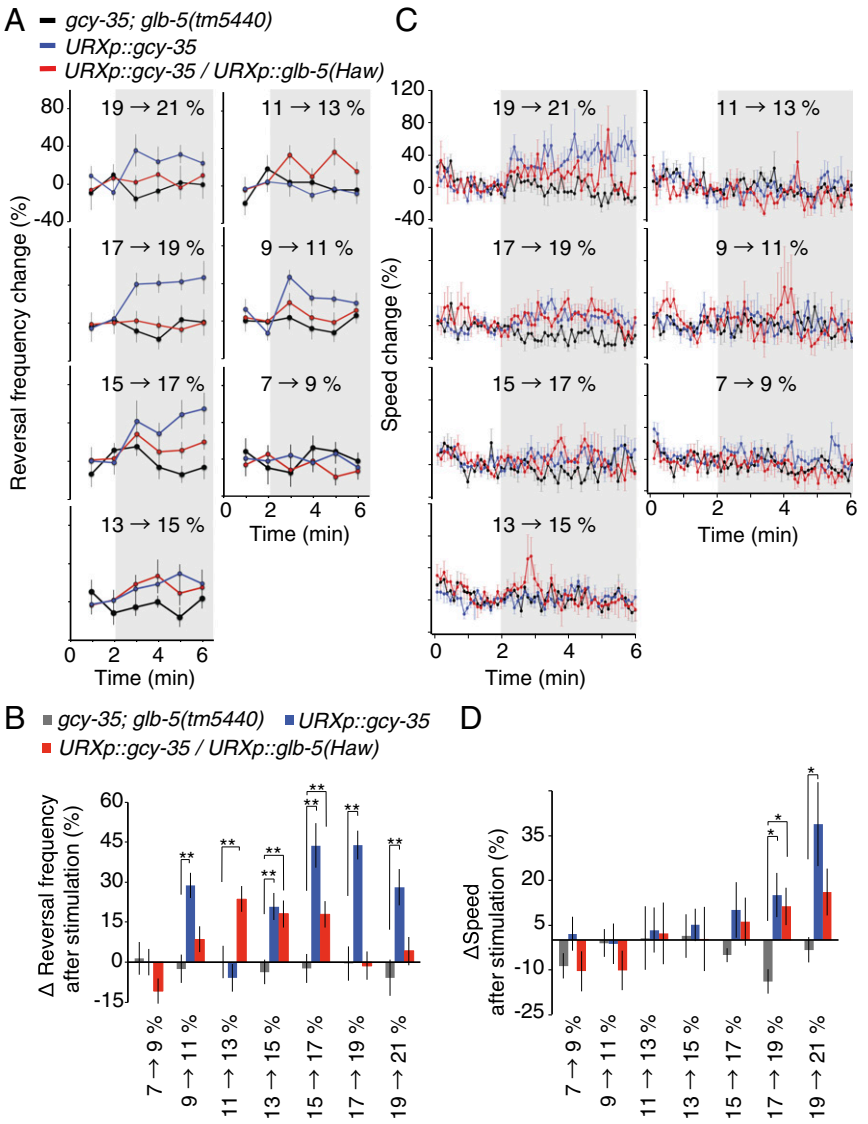

Fig. 4. The relationship between O_2 stimulus intensity and URX-dependent behavioral outputs. (*A*) Frequency of reversal behavior evoked by O_2 step stimuli in animals of the genotypes indicated. Reversal frequencies were quantified every minute. n = 15–30 animals. Bars represent SEM. (*B*) Reversal frequency evoked by step O_2 stimuli averaged over 4 min after the stimulus. Data represent mean ± SEM. (*C* and *D*) Instantaneous speed in response to step O_2 stimuli. n = 30–60 animals. Plots show mean ± SEM. (*D*) Mean speed ± SEM calculated for a 4-min interval beginning 30 s after the step stimulus. The behavior of *gcy-35(ok769); glb-5(tm5440)* animals was used as a negative control and is shown as black traces or gray bars. *$P < 0.05$, **$P < 0.01$, ANOVA with Dunnett's post hoc test.

O_2 preference (Fig. S3), we excluded other O_2-sensing neurons, including PQR and AQR, in the computational model. The model included a command neuron that randomly generates a reversal; a URX model neuron transmitted a signal to this command interneuron via an interneuron that could act as a differentiator to promote reversal (Fig. 5*A* and *Methods*). In the model, URX Ca^{2+} responses to O_2 stimuli were approximated by a nonlinear–linear–nonlinear (NLN) model (Fig. 5*A*). The parameters for the NLN model were estimated from imaging URX responses to 2% step O_2 stimuli in *glb-5(tm5440)* and *glb-5(Haw)* (Fig. S7). A single model reproduced URX Ca^{2+} responses to a variety of O_2 changes. As a result of modeling the URX responses, we acquired two sets of parameters, one for *glb-5 (tm5440)* and the other one for *glb-5 (Haw)*. The parameters for steps downstream of URX were common for *glb-5(tm5440)* and *glb-5(Haw)* virtual animals.

Having set up our model, we ran in silico aerotaxis experiments in which the position of a worm was represented as a single point (Fig. S8). These experiments showed that worms for which the URX NLN model used parameters obtained for *glb-5 (tm5440)* preferred 7–10% O_2 (Fig. 5 *B* and *C*), whereas those using *glb-5(Haw)* parameters showed broader O_2 preference, with the majority of worms preferring 7–16% O_2 (Fig. 5 *B* and *C*). The simulations made by our computational model mirrored the results of aerotaxis experiments (Figs. 1*A* and 5 *B–D*). In our initial computational model, the values for constants in the model interneuron (l) and command neuron (c) were selected arbitrarily (*Methods*). We therefore examined how changing these parameters over a wide range altered the results of our simulated aerotaxis experiments. For almost all parameter values we tested, the *glb-5(tm5440)* virtual animals preferred lower and narrower O_2 concentrations than the *glb-5(Haw)* virtual animals (Fig. S9). The distinct O_2 preferences of the two strains are thus not strongly influenced by the values of these parameters.

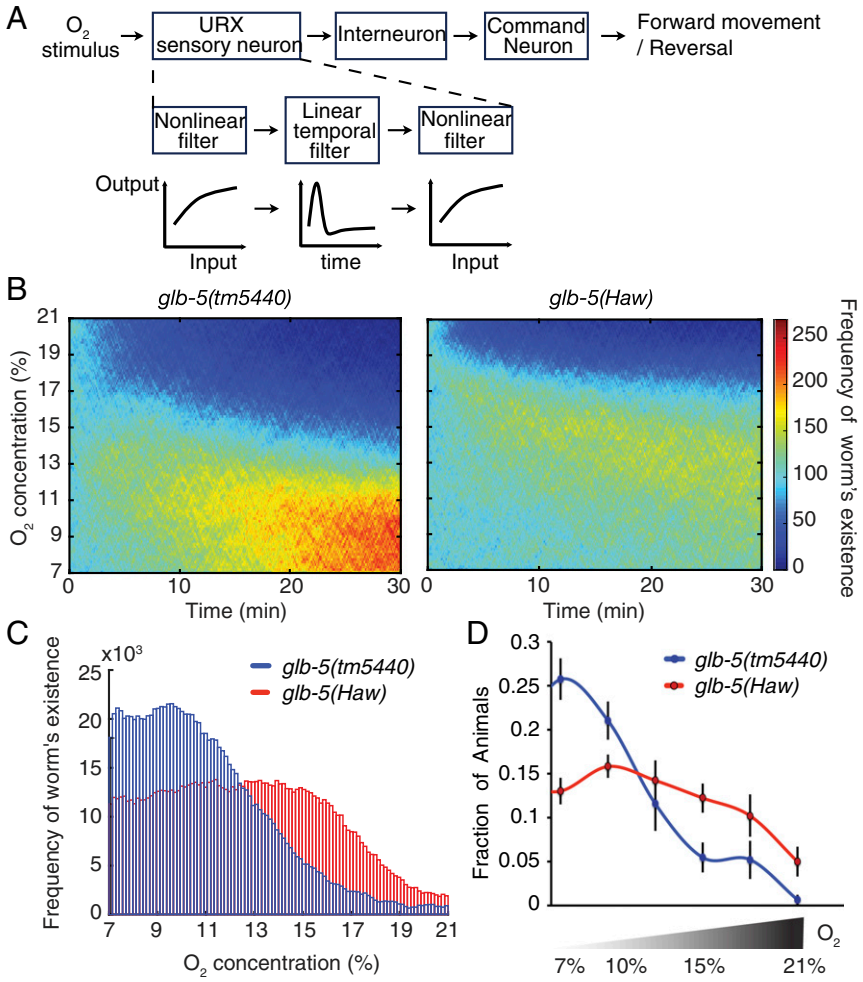

Fig. 5. A computational model that links O_2-evoked Ca^{2+} responses in URX to behavioral output. (*A*) Schematic of the computational model. (*B*) Heat map representing the location of 10000 fictive *glb-5(tm5440)* or *glb-5(Haw)* animals in a 7–21% O_2 gradient. Locations are plotted every second. (*C*) Histograms of the existence frequency of *glb-5(tm5440)* and *glb-5(Haw)* in 7–21% O_2 gradient during the last 100 s of the computational experiments shown in *B*. The fictive URX responses and reversal frequency of these model worms during aerotaxis are shown in Fig. S8. (*D*) The modified aerotaxis results from Fig. 1*A* are shown to compare results of computational experiments and those of aerotaxis experimental data.

To extend our model, we incorporated data on O_2-evoked changes in speed (Fig. 4*C* and Fig. S10), in addition to O_2-evoked changes in reversals. We found this did not substantially change the performance of *glb-5(tm5440)* and *glb-5(Haw)* in virtual aerotaxis assays. Model worms that modulated both reversals and speed in response to O_2 changes distributed similarly to animals that modulated only reversal (Fig. S11). By contrast, model worms in which changes in O_2 influenced only speed distributed almost evenly in a virtual aerotaxis chamber (Fig. S11). Thus, in our model the relationship between URX responses and reversal frequency is sufficient to account for the worm's O_2 preference in a shallow O_2 gradient.

Discussion

The neuroglobin GLB-5 changes how the URX O_2-sensing neurons encode O_2 concentration. URX sensory receptors enable *C. elegans* to avoid and escape 21% O_2. We find that URX neurons combine two putative molecular O_2 sensors, a soluble guanylate cyclase and a neuroglobin, to sculpt a sigmoidal O_2 tuning curve in which the neurons show little Ca^{2+} response to stimuli below 13% O_2, gradually increase their responsiveness above this O_2 concentration, show a sharp increase in responsiveness between 15 and 19% O_2, and approach saturation as O_2 approaches 21%. The neuroglobin GLB-5 imposes the sigmoidal function by inhibiting the O_2-evoked Ca^{2+} response in URX when O_2 levels fall below 21%. When GLB-5 is defective, the URX stimulus–response curve is shifted to lower O_2 levels and approaches saturation at 14% O_2. At a behavioral level, the effects of GLB-5 signaling are to broaden the O_2 environments preferred by *C. elegans* while maintaining avoidance of 21% O_2. If *glb-5* is defective, as in the N2 laboratory strain or the *glb-5(tm5440)* mutant, animals prefer a narrow O_2 range, from 7 to 10%. Animals with functional *glb-5* signaling distribute more broadly, from 17 to 5% O_2. It will be interesting to explore if other sensory neurons that exhibit steep sigmoidal tuning curves at defined intensity intervals achieve their properties by combining antagonistic molecular sensors. Studies of O_2 sensing in the glomus cells of the carotid bodies of mammals have implicated multiple O_2-sensing mechanisms that could act together to sculpt O_2 response features (4). Similarly, a range of CO_2/pH-responsive molecules have been identified in mammals, although whether any of the numerous CO_2/pH-responsive cells use a combination of transducers is unclear (24).

Unexpectedly, we find that the relationship between URX Ca^{2+} response (a proxy of O_2 stimulus intensity) and behavioral output is nonlinear. Whereas intermediate stimulation of URX induces animals to reverse, strong stimulation is less effective.

We have not investigated the neural mechanisms that underpin nonlinear control of reversals by URX. However, the neuroanatomical reconstructions reveal synapses from URX to both AVE interneurons that promote reversals and AVB interneurons that promote forward movement (21, 25) (wormwiring.org/), which could be differentially regulated according to URX stimulation.

Several computational models have been constructed to elucidate behavioral mechanisms underlying *C. elegans* taxis behavior (26–28). These models have been built using detailed observation of animals moving in gradients. A taxis model that incorporates quantitatively measured neural activities has not, however, been reported but is required to understand how neural signals are processed and transformed to behavior. We incorporated URX Ca^{2+} responses measured using GCaMP6s into a random walk model. These data can be extended into a more detailed model to study neural circuits of *C. elegans* at a systems level, e.g., incorporating activities of interneurons and motor neurons, to probe how encoded neural information in neural circuits are used to evoke worm behaviors.

C. elegans respond to changes in O_2 by altering both their speed and their reversal behavior. Previous work has shown that worms use a klinokinesis strategy, where frequency of reversal is changed depending on the concentration of stimuli, when aerotaxing in the absence of food (29). This strategy resembles that used by worms chemotaxing to other cues such as salts and odors (26, 30). Our quantitative experiments show that the URX oxygen sensors evoke reversals in response to O_2 stimuli that have only minor effects on speed. Our computational experiments can replicate the results of aerotaxis experiments without incorporating O_2-evoked modulation of speed. These results imply that modulation of reversal is more important than modulation of speed when *C. elegans* navigates O_2 gradients. The persistent stimulation of rapid movement when O_2 levels approach 21% may conversely enable animals to escape from the surface when animals cannot detect an O_2 gradient.

How does the GLB-5 neuroglobin alter the Ca^{2+} responses of neurons at a molecular level? Like mammalian neuroglobin (31), GLB-5 rapidly oxidizes to a ferric form at 21% O_2 (9), suggesting it could participate in ROS or redox signaling. In URX, GLB-5 colocalizes with GCY-35/GCY-36 soluble guanylate cyclases at dendritic endings (10, 16) and could potentially regulate the function of this other heme-binding protein. Our cGMP imaging did not reveal GLB-5–dependent differences in the O_2-evoked responses of URX. However, the cGMP dynamics we measured in the URX cell body were very slow compared with the Ca^{2+} response, which implies that we are measuring a highly filtered response compared with the cGMP dynamics pertaining at the cGMP-gated channel. Although we do not exclude a role for GLB-5 in regulating soluble guanylate cyclases, our data suggest that GLB-5 can alter neural responses independently of these molecules.

In summary, we find that a neuroglobin can participate in neural information processing. The *C. elegans* genome encodes a variety of other neurally expressed globins that may similarly modify neural function (8). It would be interesting to investigate whether neuroglobin alters information processing in vertebrate neural circuits.

Methods

Strains. Animals were grown at 22–23 °C under standard conditions on Nematode Growth Medium (NGM) seeded with *Escherichia coli* OP50 (32). Strains used are listed in *Supporting Information*.

Neural Imaging.

Immobilized animals. Animals expressing GCaMP6s or cGi500 were glued to agarose pads (2% in M9 buffer) using Dermabond tissue adhesive (Ethicon), with the nose and tail immersed in *E. coli* OP50 unless otherwise indicated. Glued worms were covered with a polydimethylsiloxane (PDMS) microfluidic chamber, as described previously (12), and imaged using a 40× C-Apochromat lens on an inverted microscope (Axiovert; Zeiss) equipped with a Dual View emission splitter (Photometrics) and a Cascade II 512 electron multiplying charge coupled device (EMCCD) camera (Photometrics). The filters used were as follows: GCaMP6s/mCherry, ex480/15 and 565/15 nm, di525/25 and 625/45 nm, em520/30 nm, em630/50 nm, and di565 nm; and YFP-CFP FRET, ex430/20 nm, di450 nm, em480/30 nm, em535/40 nm, and di505 nm. Fluorescent images were captured at 1 frame per second (fps) with 2 × 2 or 1 × 1 binning using MetaMorph acquisition software (Molecular Devices). Data analysis used MATLAB (MathWorks) and Igor Pro (WaveMetrics). All time-lapse imaging data were denoised using binomial smoothing (Gaussian filter).

Delivery of gas stimuli. Humidified gas mixtures of defined composition were delivered using a PHD 2000 Infusion syringe pump (Harvard Apparatus). The flow rate was 1.0 mL/min for all ramp stimuli and 2.0 mL/min for all step stimuli. Syringes containing gas mixtures were connected to PDMS chambers via polyethylene tubing and Teflon valves (AutoMate Scientific). A custom-built frame counter switched the valves at precise time points using transistor–transistor logic pulses from the camera. To create the ramp stimulation, we used backlash air from the outlet of the PDMS chamber. O_2 stimuli in chambers were measured using an O_2 probe (Oxygen Sensor Spots PSt3; PreSens).

Behavioral Assays. Aerotaxis assays were performed as described previously (11); animal positions were noted 25 min into the assay. Briefly, rectangular PDMS chambers (33 × 15 × 0.2 mm) connected at either end to syringe pumps delivering the indicated gas concentration were placed over 50–100 worms on a 9-cm NGM agar plate with food (*E. coli* OP50). The distribution of worms was recorded by counting animals in each of nine equal areas of the chamber.

To measure behavioral responses to step O_2 stimuli, five adult hermaphrodites were placed on NGM plates seeded 36–40 h earlier with 20 μL of *E. coli* OP50 grown in 2× TY medium. To create a behavioral arena with a defined atmosphere, we placed a PDMS chamber (1 × 1 × 0.2 cm) on top of the worms, with inlets connected to a PHD 2000 Infusion syringe pump (Harvard Apparatus), and delivered humidified gas mixtures of defined composition at a flow rate of 3.0 mL/min. Videos were captured at 2 fps using FlyCapture software (Point Gray) on a Grasshopper camera (Point Gray) mounted on a Leica M165FC stereo microscope. Videos were analyzed using custom-written MATLAB software to calculate instantaneous speed. Instantaneous speed data were denoised by binning over 6 s. Reversal frequency was counted manually. If the posterior and anterior tips of a worm's body moved backward until the worm stopped, this behavior was counted as one reversal; such events were often followed by turns.

Computational Experiments and Modeling. In the computational model, a worm was represented as a single point in a virtual field that represented an O_2 gradient in our experimental 18 mm (W) × 15 mm (L) aerotaxis chamber. O_2 levels in the virtual chamber varied from 7% at W = 0 mm to 21% at W = 18 mm. The worm moved forward either at constant (~0.05 mm/s) or at variable speed. For iterations when speed varied according to O_2 concentration at the animal's position we acquired parameters for speed by performing curve fitting with a Hill equation using the speed data shown in Fig. 4*C* (Fig. S11 *B* and *C*). The trend in an averaged time series was identified and removed based on the gradient of the time series. If the worm reached the edge of the chamber, the direction of forward movement was reflected. The model worm has three modules that correspond to the sensory neuron (URX), an interneuron, and a command neuron (Fig. 5*A*). The information signal about O_2 level is transmitted from the sensory neuron to the command neuron through the interneuron. The activation of the command neuron causes a worm to start reversing. Reversals are expressed as a change in the direction of locomotion in the model. The locomotion direction after the reversal was randomly chosen from a uniform distribution $(0,2\pi)$ because experimentally measured reversals contain turning events. We assumed that the relationship between URX responses and reversal frequency was approximately linear in our model. This applies because animals in the virtual O_2 gradient, like those in a real-life aerotaxis assay, do not encounter large step O_2 stimuli.

The dynamics of the sensory circuit were represented by an NLN model. The NLN model consisted of two nonlinear static filters and a linear temporal filter. O_2 stimulation was first converted by the input nonlinear filter, processed by the temporal filter, then converted by the output nonlinear filter. The nonlinear filter $f(x)$ was expressed using a Hill equation,

$$f(x) = x^n / (x^n + x_0^n),$$

where x_0 and n were the parameters that defined the range and strength of the nonlinearity of the filter, respectively. For convenience, the input and

output nonlinear filter are hereafter denoted as f_{in} and f_{out}, respectively. The linear temporal filter K has a 361 sample length ($t = 0,1, \ldots 360$) and satisfies

$$y = UK,$$

where U and y are the input and output time courses of the temporal filter, respectively. This typical expression of a temporal filter should be expanded because our dataset has multiple time courses (multidose). If O_2 concentration is left as x, U can be written as

$$U = [\,U_1 \quad U_2 \quad \ldots \quad U_{d\max}\,]^T,$$

$$U_d = f_{in}\left(\begin{bmatrix} x_d(0-t_{\max}) & x_d(1-t_{\max}) & \ldots & x_d(0) \\ x_d(1-t_{\max}) & x_d(2-t_{\max}) & \ldots & x_d(1) \\ \vdots & \vdots & \ddots & \vdots \\ x_d(0) & x_d(1) & \ldots & x_d(t_{\max}) \end{bmatrix}\right),$$

where $x_d(t)$ corresponds to the O_2 concentration at time t of dth step stimulation and $x_d(t<0)$ is replaced by $x_d(0)$. y can be expressed as

$$y = [\,y_1 \quad y_2 \quad \ldots \quad y_{d\max}\,]^T,$$

$$y_d = [\,y_d(0) \quad y_d(1) \quad \ldots \quad y_d(t_{\max})\,]^T,$$

where $f_{out}[y_d(t)]$ corresponds to the response of the sensory neuron at time t in response to dth oxygen step stimulation. The linear temporal filter K can be obtained by evaluating

$$K = (U^T U)^{-1} U^T y\,.$$

For denoising, singular value decomposition was applied, and the largest 100 components were used. To find the value of parameters of nonlinear filters, the Nelder–Mead simplex optimization method was used, and the sum of the square difference between $f_{out}[y_d(t)]$ and corresponding experimental Ca^{2+} responses of URX were minimized. Because this optimization was done separately for *glb-5(Haw)* and *glb-5(tm5440)*, we obtained two parameter sets for the NLN model.

The interneuron and command neurons were designed as described below. Because the worms show random reversals, the command neuron should be randomly activated. Furthermore, because the basal URX Ca^{2+} response (i.e., before stimulation of 2% change of oxygen) depends on the basal concentration of O_2 but basal reversal frequency does not, the model should contain a temporal differentiation functionality. Therefore, the activity of interneuron $g(t)$ was modeled as

$$g(t) = f_{out}[y_d(t)] - \sum_{\tau=1}^{l} f_{out}[y_d(t-\tau)]/l,$$

where l is a lag constant and was initially fixed as 11 and then varied (Fig. S9). The activity of command neuron is positive when

$$r < b[1 + g(t)c],$$

where b is the basal reversal frequency that is computed from experimental data, c is the coefficient of the effect of O_2 stimulation, and r is a uniformly distributed random number between 0 and 1. b and c were fixed to 0.0723 (reversal frequency per 1 s before a stimulation is given) and 3, respectively; c was subsequently varied (Fig. S9). Note that the parameters of interneuron and command neuron (l, b, and c) are independent of the *glb-5* genotype.

ACKNOWLEDGMENTS. We thank the National Bioresource Project (Japan) for strains; W. Schafer and Y. Iino for plasmids; and I. Beets, L. Fenk, T. Tomida, and S. Laughlin for comments on the manuscript. This work was supported by the Medical Research Council (MC_U105178786) and the European Research Council (AdG 269058) (to M.d.B.); the Uehara Memorial Foundation (S.O.); Grants-in-Aid for Young Scientists (B) (26830006 to Y.T.); and Grant-in-Aid for Scientific Research on Innovative Areas (16H01418 "Resonance Bio" and 17H05970) from the Ministry of Education, Culture, Sports, Science and Technology of Japan (to Y.T.).

1. Butts DA, Goldman MS (2006) Tuning curves, neuronal variability, and sensory coding. *PLoS Biol* 4:e92.
2. Dayan P, Abbott LF (2005) *Theoretical Neuroscience: Computational and Mathematical Modeling of Neural Systems*, Computational Neuroscience Series (MIT Press, Cambridge, MA).
3. Ward JP (2008) Oxygen sensors in context. *Biochim Biophys Acta* 1777:1–14.
4. López-Barneo J, et al. (2016) Oxygen sensing by the carotid body: Mechanisms and role in adaptation to hypoxia. *Am J Physiol Cell Physiol* 310:C629–C642.
5. Burmester T, Hankeln T (2014) Function and evolution of vertebrate globins. *Acta Physiol (Oxf)* 211:501–514.
6. Burmester T, Weich B, Reinhardt S, Hankeln T (2000) A vertebrate globin expressed in the brain. *Nature* 407:520–523.
7. Burmester T, Hankeln T (2009) What is the function of neuroglobin? *J Exp Biol* 212: 1423–1428.
8. Tilleman L, et al. (2011) Globins in Caenorhabditis elegans. *IUBMB Life* 63:166–174.
9. Persson A, et al. (2009) Natural variation in a neural globin tunes oxygen sensing in wild Caenorhabditis elegans. *Nature* 458:1030–1033.
10. McGrath PT, et al. (2009) Quantitative mapping of a digenic behavioral trait implicates globin variation in C. elegans sensory behaviors. *Neuron* 61:692–699.
11. Gray JM, et al. (2004) Oxygen sensation and social feeding mediated by a *C. elegans* guanylate cyclase homologue. *Nature* 430:317–322.
12. Busch KE, et al. (2012) Tonic signaling from O_2 sensors sets neural circuit activity and behavioral state. *Nat Neurosci* 15:581–591.
13. Cheung BH, Arellano-Carbajal F, Rybicki I, de Bono M (2004) Soluble guanylate cyclases act in neurons exposed to the body fluid to promote *C. elegans* aggregation behavior. *Curr Biol* 14:1105–1111.
14. Couto A, Oda S, Nikolaev VO, Soltesz Z, de Bono M (2013) In vivo genetic dissection of O2-evoked cGMP dynamics in a Caenorhabditis elegans gas sensor. *Proc Natl Acad Sci USA* 110:E3301–E3310.
15. Prabhakar NR, Semenza GL (2015) Oxygen sensing and homeostasis. *Physiology (Bethesda)* 30:340–348.
16. Gross E, et al. (2014) GLOBIN-5-dependent O2 responses are regulated by PDL-1/PrBP that targets prenylated soluble guanylate cyclases to dendritic endings. *J Neurosci* 34: 16726–16738.
17. Chen TW, et al. (2013) Ultrasensitive fluorescent proteins for imaging neuronal activity. *Nature* 499:295–300.
18. Cheung BH, Cohen M, Rogers C, Albayram O, de Bono M (2005) Experience-dependent modulation of C. elegans behavior by ambient oxygen. *Curr Biol* 15: 905–917.
19. Rogers C, Persson A, Cheung B, de Bono M (2006) Behavioral motifs and neural pathways coordinating O2 responses and aggregation in C. elegans. *Curr Biol* 16: 649–659.
20. Russwurm M, et al. (2007) Design of fluorescence resonance energy transfer (FRET)-based cGMP indicators: A systematic approach. *Biochem J* 407:69–77.
21. White JG, Southgate E, Thomson JN, Brenner S (1986) The structure of the nervous system of the nematode *Caenorhabditis elegans*. *Philos Trans R Soc Lond B Biol Sci* 314:1–340.
22. Macosko EZ, et al. (2009) A hub-and-spoke circuit drives pheromone attraction and social behaviour in C. elegans. *Nature* 458:1171–1175.
23. Laurent P, et al. (2015) Decoding a neural circuit controlling global animal state in C. elegans. *eLife* 4:4.
24. Huckstepp RT, Dale N (2011) Redefining the components of central CO2 chemosensitivity–towards a better understanding of mechanism. *J Physiol* 589:5561–5579.
25. Chalfie M, et al. (1985) The neural circuit for touch sensitivity in *Caenorhabditis elegans*. *J Neurosci* 5:956–964.
26. Pierce-Shimomura JT, Morse TM, Lockery SR (1999) The fundamental role of pirouettes in Caenorhabditis elegans chemotaxis. *J Neurosci* 19:9557–9569.
27. Ghosh DD, et al. (2016) Neural architecture of hunger-dependent multisensory decision making in C. elegans. *Neuron* 92:1049–1062.
28. Izquierdo EJ, Lockery SR (2010) Evolution and analysis of minimal neural circuits for klinotaxis in Caenorhabditis elegans. *J Neurosci* 30:12908–12917.
29. Hums I, et al. (2016) Regulation of two motor patterns enables the gradual adjustment of locomotion strategy in Caenorhabditis elegans. *eLife* 5:5.
30. Iino Y, Yoshida K (2009) Parallel use of two behavioral mechanisms for chemotaxis in Caenorhabditis elegans. *J Neurosci* 29:5370–5380.
31. Dewilde S, et al. (2001) Biochemical characterization and ligand binding properties of neuroglobin, a novel member of the globin family. *J Biol Chem* 276:38949–38955.
32. Sulston J, Hodgkin J (1988) *The Nematode Caenorhabditis elegans*, ed Wood WB (CSHL Press, Cold Spring Harbor), pp 587–606.